Journal of Magnetic Resonance 198 (2009) 137–145

Contents lists available at ScienceDirect

Journal of Magnetic Resonance

journal homepage: www.elsevier.com/locate/jmr

MRI dynamic range and its compatibility with signal transmission media

Refaat E. Gabr [a,b], Michael Schär [a,c], Arthur D. Edelstein [d], Dara L. Kraitchman [a], Paul A. Bottomley [a,b], William A. Edelstein [a,*]

[a] Division of MR Research, Department of Radiology, Johns Hopkins School of Medicine, 600 N Wolfe St., Park 328, Baltimore, MD, USA
[b] Department of Electrical and Computer Engineering, The Johns Hopkins University, Baltimore, MD, USA
[c] Philips Healthcare, Cleveland, OH, USA
[d] Department of Physics, University of California, Berkeley, CA, USA

ARTICLE INFO

Article history:
Received 19 August 2008
Revised 10 January 2009
Available online 4 February 2009

Keywords:
Dynamic range
Magnetic resonance imaging
MRI
Magnitude image
Fiber optic link
Wireless link
Signal-to-noise ratio

ABSTRACT

As the number of MRI phased array coil elements grows, interactions among cables connecting them to the system receiver become increasingly problematic. Fiber optic or wireless links would reduce electromagnetic interference, but their dynamic range (DR) is generally less than that of coaxial cables. Raw MRI signals, however, have a large DR because of the high signal amplitude near the center of k-space. Here, we study DR in MRI in order to determine the compatibility of MRI multicoil imaging with non-coaxial cable signal transmission. Since raw signal data are routinely discarded, we have developed an improved method for estimating the DR of MRI signals from conventional magnitude images. Our results indicate that the DR of typical surface coil signals at 3 T for human subjects is less than 88 dB, even for three-dimensional acquisition protocols. Cardiac and spine coil arrays had a maximum DR of less than 75 dB and head coil arrays less than 88 dB. The DR derived from magnitude images is in good agreement with that measured from raw data. The results suggest that current analog fiber optic links, with a spurious-free DR of 60–70 dB at 500 kHz bandwidth, are not by themselves adequate for transmitting MRI data from volume or array coils with DR ~90 dB. However, combining analog links with signal compression might make non-coaxial cable signal transmission viable.

Supported by Grants R01 EB007829 (formerly RR15396).

1. Introduction

The number of coils in magnetic resonance imaging (MRI) phased arrays has been steadily increasing as manufacturers add receive channels and MRI researchers pursue increased spatial resolution and effective parallel imaging. Commercial and experimental arrays with 32, 64, 96 and 128 coils have been reported (e.g. [1–6]). Electrical interactions among these coils and cable connections to the system interface, and also between cables and the applied RF and gradient fields, can be problematic. A number of research groups have experimented with fiber optic or wireless links between MRI coils and the MRI system [7–21]. These alternative signal links can potentially reduce the complexity, electromagnetic interference and interactions of traditional coaxial cable connections.

Optical or wireless links may have limited dynamic range (DR) compared to electric conductors. It is therefore important to accurately determine this parameter both in the MR signal and in the signal link. Some estimates of human MR signal DR have been very high: 125 dB [16], 150 dB [22] and 193 dB [23]. Thus, there is concern whether MRI signals can be faithfully carried by non-coaxial cable signal links.

However, these DR figures have generally been derived assuming extreme conditions, for example, volume coils fully filled by water or solid biological tissue samples. But surface coils in a multicoil array—the most appropriate arrangement for non-coaxial cable transmission—have much smaller sensitive regions than volume coils, and the body is not solid tissue. A single measurement by He et al. on a phantom at 0.3 T, for example, gave a much lower DR of 76 dB [24].

DR can be directly measured from the (k-space) input signal, but these data are routinely discarded in practice. When the raw data are Fourier transformed (FT) and processed by the scanner, phase information is lost and only magnitude images are retained. Obtaining the signal DR from magnitude images could therefore provide a practical way of measuring DRs for classes of images (surface coils, volume coils, etc.) and for different pulse sequences from those studies when only magnitude images have been preserved. It is therefore desirable to have a way to accurately measure DR from magnitude images, which can then be applied to the usually vast supply of existing MRI data, thus avoiding the need for costly repeat studies.

In this work, we consider theoretical aspects of DR in MRI and measure DRs for several coil arrangements using common pulse

* Corresponding author. Fax: +1 410 614 1977.
E-mail address: w.edelstein@gmail.com (W.A. Edelstein).

1090-7807/$ - see front matter © 2009 Elsevier Inc. All rights reserved.
doi:10.1016/j.jmr.2009.01.037

sequences. Special attention is given to surface coil elements of multicoil arrays used for head, spine, and cardiac MRI at 3 T. For each imaging experiment, the DR is determined from the raw signal and compared to DR estimates derived from the resulting magnitude images. We also study the feasibility of using fiber optic and wireless links to transmit MRI signals.

2. Theory

2.1. Dynamic range, digitization and digitization noise

The DR of a signal is the power ratio of its largest to its smallest significant values. DR is commonly expressed in decibels,

$$\mathrm{DR} = 20 \cdot \log_{10}\left(\frac{2S_{\max}}{\varepsilon}\right) \tag{1}$$

where $S_{\max}$ is the largest signal amplitude and ε is the smallest amplitude—signal or noise—to be measured. This ratio determines how many bits are needed for an analog-to-digital converter (ADC) to produce a digital representation of the signal. It also specifies the DR requirements of channels transmitting this signal. The factor of two in the parentheses accounts for the fact that the signal can be positive or negative.

The amplitude DR of an J-bit ADC is $2^J - 1 \approx 2^J$ for large J. A crucial question when digitizing a signal is the size of the digitization interval, i.e. how low should we go in preserving the noise, in order that the signal measurement not be degraded. The minimum number of bits J required to satisfy the DR requirement of the input signal (Eq. (1)) is given by

$$\mathrm{DR} = 20 \cdot \log_{10}(2^J) \tag{2}$$

where DR is in dB.

Solving Eq. (2) for J gives us

$$J = \frac{\mathrm{DR}}{6.02} \tag{3}$$

Eq. (2) assumes that one bit is used to represent the root mean square (rms) noise. As is explained in Appendix A, this choice adds 0.35 dB to the system noise figure.

2.2. The dynamic range in MRI: k-space and image

We now examine the relationship between the DR found from k-space data and DR derived from the corresponding image. Every method of traversing k-space to form an image—spin warp, projection reconstruction, spiral, etc.—passes through (or very near) $\mathbf{k} = 0$. At $\mathbf{k} = 0$, all contributing spins in the imaged section—slice or three-dimensional (3D) volume—are approximately in phase, and the signal is maximized. The DR is thus the ratio of this maximum signal to the rms noise.

The image is the FT of the k-space data. Since the 2D or 3D FT used to produce an image is separable, we need only consider the 1D FT; extension to higher dimensions is straightforward. The discrete 1D FT pair is given by

$$\begin{aligned} A_n &= \frac{1}{\sqrt{N}} \sum_{m=0}^{N-1} S_m e^{-j(\frac{2\pi n}{N})m} \\ S_m &= \frac{1}{\sqrt{N}} \sum_{n=0}^{N-1} A_n e^{j(\frac{2\pi m}{N})n} \end{aligned} \tag{4}$$

where $j = \sqrt{-1}$. We adopt the convention that S_m is the mth k-space signal sample, and A_n is the true noise-free image intensity of the nth voxel and N is the total number of points in the FT. With the $\sqrt{N}$ normalization, noise in k-space has the same amplitude as noise in the image.

It is readily apparent that S_0, the peak of the signal, is the sum of all image voxel values.

$$S_0 = \frac{1}{\sqrt{N}} \sum_{n=0}^{N-1} A_n \tag{5}$$

for a single traversal through K-space. Dividing by the noise standard deviation, σ

$$\begin{aligned} \mathrm{DR} &= 20 \cdot \log_{10}(2S_0/\sigma) = 20 \cdot \log_{10}\left(\frac{2}{\sqrt{N}} \sum_{n=0}^{N-1} \frac{A_n}{\sigma}\right) \\ &= 20 \cdot \log_{10}\left(\frac{2}{\sqrt{N}} \sum_{n=0}^{N-1} SNR_n\right) \end{aligned} \tag{6}$$

Thus the DR is derived from the sum of image voxels signal-to-noise ratio (SNR) normalized by $\sqrt{N}$ for an image generated from a single traversal of k-space. In order to correctly estimate DR from an image generated using multiple acquisitions, the image voxel SNR must be divided by the square root of the number of signals averaged $\sqrt{NEX}$. Using the mean voxel SNR ($\overline{SNR}$), the DR estimate then becomes

$$\mathrm{DR} = 20 \cdot \log_{10}(2\sqrt{N} \cdot \overline{SNR}/\sqrt{NEX}) \tag{7}$$

Many useful conclusions can be drawn from Eq. (6). First, any parameter that globally affects the SNR will similarly affect DR. For example, MRI/MRS nuclei other than protons (1H)—like phosphorus (^{31}P), carbon (^{13}C) or sodium (^{23}N)—have low SNR and hence low DR. Similarly, field strength, scan geometry, contrast mechanisms and any other factors affecting SNR will affect DR in the same manner.

Second, it is the sum of all SNR, not the local SNR, that determines the DR. Although a surface coil has a high SNR in its vicinity, the limited sensitive region of the coil may result in a smaller SNR sum, and consequently smaller DR, than would be obtained for a volume coil with a uniform sensitivity and larger sensitive region. As surface coils get smaller, so does the DR. In Section 2.4 and Appendix B we analyze DR scaling for a circular loop coil.

MRI DR can be very high, especially for 3D acquisitions. If the resolution of the ADC is less than the signal DR, distortion or extra noise may result, especially for high-resolution imaging [25]. Several approaches have been proposed to make the MRI signal DR compatible with the ADC DR. These include: decreasing the DR of the MR signal using, for example, nonlinear gradient pulses [26,27], special pulse sequences [28], or nonlinear signal compression [29]; enhancing the effective DR of the ADC by sampling the signal at higher than the Nyquist rate, thereby reducing ADC quantization noise [30]; and k-space location-dependent amplification in which measurements made with different gain settings are rescaled and assembled to enable the ADC to cover a DR larger than the native ADC DR [25,31,32].

2.3. Deriving DR from magnitude images

To obtain the DR from a magnitude image, we need to calculate the highest input k-space signal and k-space noise power. The noise in the input signal can be computed from noise measured in signal-free regions of the magnitude image [33,34]. However, in order to estimate the highest signal in k-space using Eq. (5), the true voxel amplitude A_n must be estimated from the noisy image. Given Gaussian noise with standard deviation σ in the real and imaginary channels of the complex image, the *magnitude* image data follows a Rician probability distribution [35]

$$p(M; A, \sigma) = \frac{M}{\sigma^2} \exp\left[-\frac{(M^2 + A^2)}{2\sigma^2}\right] \cdot I_0\left(\frac{A \cdot M}{\sigma^2}\right) \tag{8}$$

where M is the measured (noisy) value of the image amplitude in any single voxel, A is the true noiseless amplitude of that voxel and I_0 is the modified zeroth-order Bessel function of the first kind.

At high SNR values ($A \geqslant 3\sigma$), the data becomes approximately Gaussian, and a good estimate of the true image amplitude can be derived from the apparent image amplitude by [35,36]

$$A \approx \sqrt{M^2 - \sigma^2} \tag{9}$$

Thus, the actual image amplitude is slightly less than the apparent amplitude because of noise. At SNR ~ 0, the image amplitude values comprise a Rayleigh distribution whose average value is 1.253 times σ. At low SNR ($A < 3\sigma$), where image and noise amplitudes are comparable, there is no good estimate of the true image amplitude.

Previous attempts to determine true voxel amplitudes in magnitude images [35,37–44] tend to overestimate A when SNR is low. Examples of these calculations include the formula of Gudbjartsson and Patz [35]

$$A \approx \sqrt{|M^2 - \sigma^2|} \tag{10}$$

and that suggested by Andersen [43]

$$A \approx \begin{cases} \sqrt{M^2 - \sigma^2} & M \geqslant \sigma \\ 0 & M < \sigma \end{cases} \tag{11}$$

It is apparent that it is possible to end up with a value of DR that is too high when derived from a magnitude image containing extensive low signal regions where noise makes substantial contributions to the summation in Eq. (6).

We therefore generalize Eq. (10) by inserting a scaling factor that gradually changes as a function of SNR. This scaling is important where the image amplitude is low or zero. An unbiased estimate of the DR requires that positive and negative contributions of the image amplitude be allowed. Our generalized formula is

$$A(M,\sigma) \approx \mathrm{sgn}(M^2 - a(M;\sigma)\cdot\sigma^2) \times \sqrt{|M^2 - a(M;\sigma)\cdot\sigma^2|} \tag{12}$$

where sgn denotes the signum function and

$$a(M;\sigma) = \begin{cases} 1 & M/\sigma > 3 \\ 2.2 - (0.4M/\sigma) & M/\sigma \leqslant 3 \end{cases} \tag{13}$$

This choice of $a(M;\sigma)$ reduces to the formula in Eq. (8) for image regions with high SNR. The value of $a(M;\sigma)$ for $M/\sigma \leqslant 3$ is chosen to minimize the error in the amplitude estimate for regions containing mostly noise.

Inserting Eq. (12) into Eq. (6) results in the following image domain DR estimate,

$$\mathrm{DR} = 20\cdot\log_{10}\left(\frac{2}{\sigma\sqrt{N\cdot NEX}}\sum_{n=0}^{N-1}\left[\mathrm{sgn}(M_n^2 - a(M_n;\sigma)\sigma^2) \times\sqrt{|M_n^2 - a(M_n;\sigma)\sigma^2|}\right]\right) \tag{14}$$

Where M_n is the image amplitude in the nth voxel. This formula was found to give fairly accurate values for the DR in simulations of noisy magnitude images.

Eq. (12) is compared to other estimators in Fig. 1. Numerical simulations were performed to test the average performance of 10,000 samples with different SNR levels. No formula works perfectly at all SNR levels. However, Eq. (12) gives good DR results because it does well in noisy—i.e. background and low-sensitivity—image regions, which are common in real MR images, especially those made using surface coils.

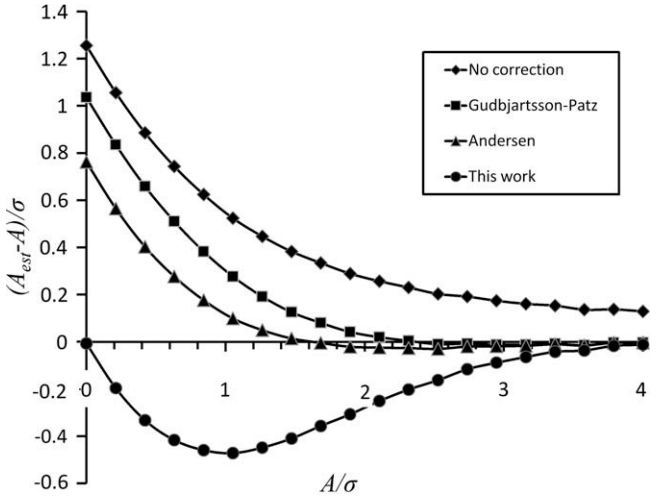

Fig. 1. Numerical simulation of the relative difference between the estimated signal amplitude A_{est} and the actual amplitude A normalized by the noise standard deviation σ as a function of the SNR, A/σ. All estimators have systematic errors at low SNR. The estimators compared here are the Gudbjartsson–Patz formula [35], Andersen's approach [43] and Eq. (12) in this work. Our estimator optimizes performance near $A = 0$ and thereby eliminates false contributions to DR from large noisy image regions.

2.4. Dynamic range scaling for circular loop coils

Once we determine DRs for a number of circular loop coils, it is useful to be able to scale the DR as a function of loop radius. We assume for this calculation a circular loop coil whose noise is sample-dominated. Including coil losses would decrease the DR slightly, i.e. by a few dB. The coil is placed against a uniform half-plane sample. In order to calculate the DR, we must calculate noise power and total signal induced in the coil as a function of the coil radius a. This calculation is detailed in Appendix B, with the result that

$$\mathrm{DR} \propto \log_{10}(a) \tag{15}$$

Reducing the coil radius by a factor of two will thus result in a 3 dB drop in DR.

3. Experiments

Head, spine, and cardiac images of a normal volunteer were acquired on a Philips Achieva 3T system using a birdcage coil and 8-channel multicoil array for the head and 6-channel multicoil arrays for spine and cardiac studies. The scanner receiver chain employs profile-dependent amplification where extra attenuation is added as the data acquisition approaches the center of the k-space. Digitization is done with a 14-bit ADC with sampling frequency of 80 MHz. For a signal bandwidth of 500 kHz, this results in additional $(1/2)\cdot\log_2[(80\ \mathrm{MHz}/500\ kHz)/2] = 3.16$ bits, or a total of ~17-bits effective ADC resolution. This is sufficient to handle MR signals with DR up to 103 dB, satisfying the requirements for the range of DR measured in this study.

Spin echo (SE), gradient recalled echo (GRE), inversion recovery (IR) and balanced steady-state free precession (SSFP) MR scans were performed in order to assess the DR of the MR signal in common clinical scan protocols and to validate the DR estimator from magnitude images. A Philips head phantom (20 cm OD × 12.5 cm long, 770 mg $CuSO_4{\cdot}5H_2O$/L H_2O, 7 ml of 1% Arquad solution, 0.1 N H_2SO_4) was used with the birdcage coil. A second Philips phantom (40 cm OD × 12.5 cm long, mineral oil) was used with the cardiac array. Typical 2D and 3D pulse sequences were applied with clinical protocol parameters.

Raw signals were examined for each coil in multicoil arrays and DRs were calculated as twice the k-space peak value divided by the noise standard deviation determined from a separate noise acquisition. The noise acquisition was a few thousand signal samples recorded without radiofrequency excitation. The DR was then computed from each magnitude image using Eq. (14).

It is a common practice that the FOV and the receiver bandwidth is increased (usually doubled) in the readout direction to reduce the effect of aliasing artifacts, especially if the imaged object is larger than the prescribed FOV. After reconstruction the image is truncated back to the original FOV.

However, the DR derived from the image will be affected by discarding part of the image. When the FOV is doubled but the object lies entirely in the prescribed FOV, the discarded half of the image contains only noise. Then the DR calculated from the truncated image is 3.01 dB higher than what we would measure from the full image or directly from the signal. This can be understood from Eq. (7) where truncation of the image doubles the average voxel SNR while the reduced number of voxels contributes only a $\sqrt{2}$ reduction in DR. Thus the net effect is a factor of $\sqrt{2}$ (or 3.01 dB) increase in DR.

To account for this effect, 3.01 dB was subtracted from the image DR. All signal and image DR analysis was performed using Matlab (The MathWorks, Natick, MA). Statistical analysis was carried out using Excel (Microsoft, Seattle, WA).

4. Results

The DR calculated from the raw k-space signal is summarized in Table 1 and plotted in Fig. 2 for different coil types and experimental conditions. There are a wide variety of scan types, with varying bandwidths, which illustrate the range of DRs that can occur in practice.

The cardiac and spine multicoil arrays have maximum DRs for the human images of 72.4 dB and 74.5 dB, respectively. The multicoil head array and the birdcage head coil produced maximum human DRs of 87.6 and 83.0 dB. Except for 3D phantom data, all DR measured in the signal space have DR less than 89 dB. All 2D human images have DR below 82 dB while 3D images have DR of up to 88 dB.

DRs calculated from the raw k-space data (DR_k) are compared in Fig. 3 to magnitude image DRs (DR_I) for different coils and imaging targets. Data from humans and phantoms are labeled differently as well as data from 2D and 3D protocols. The good agreement between DR_k and DR_I is evidenced by the small bias of only 1.8 dB derived using Bland-Altman analysis [45] of this data (Fig. 3B). For all

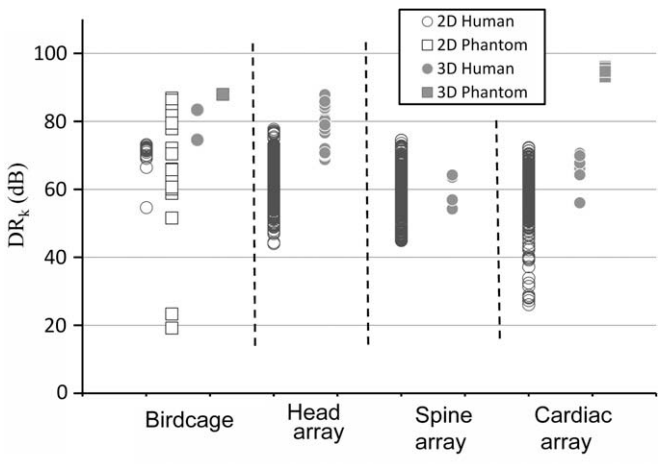

Fig. 2. The DR derived from the k-space signal, DR_k, calculated for 1806 images/volumes in different coils.

data points, 95% of the DR_I data lies between −3.0 and 6.5 dB of DR_k.

The DR_I values can be considerably higher than the k-space DR_ks for 3D GRE images (3D data from Fig. 3 are plotted here separately in Fig. 4). This is because GRE scans, without a refocusing 180° pulse, are prone to small phase errors that reduce the DR but do not affect the image. Since the image-forming magnitude operation eliminates the phase, it overestimates DR, especially in 3D scans where a larger number of voxels are accumulated in the summation. So the 3D GRE data signal DR is, on average, 6.8 dB lower than DR estimated from the 3D images. On the other hand, lower DR_I may result if the image plane or volume has large areas with very low SNR, or when the noise region is contaminated with signal artifacts.

5. Discussion

5.1. Dynamic range theory and measurement

Our proposed method for deriving DR from magnitude image data, as encapsulated by Eq. (14), allows calculation of DR from images whose raw k-space data have been discarded, as is typically the case. We measured the DR in 3 T MRI data acquired at receiver bandwidths of about 30–500 kHz from the human head and body using a range of commercial volume and array detectors and stan-

Table 1
Summary of k-space measurements and maximum DRs.

Coil	Size of elements [cm]	Images	Receiver BW [min–max] kHz	Maximum DR, 2D or 3D (dB)
Head Birdcage	25(L) × 30(D)	SE, 2D, 21 head images SE, 3D, 1 head image GRE, 3D, 1 head image	[44–75]	83.0
		SE, 2D, 22 phantom images. SE, 3D, 1 phantom image.	[70–71]	89.5
Head array	8 Rectangular loop coils 17.2 × 10.0	SE, 2D, 736 head images SE 3D, 8 head images GRE 3D, 24 head images IR 2D, 272 head images	[29–200]	87.6
Spine array	6 Square loop coils: 15.5 × 15.5 6 Fig-8 coils: 14.8 × 30.6 Fig-8 coil spacing: 4.00	SE 2D, 362 spine images GRE 3D, 4 spine images	[29–355]	74.5
Cardiac array	3 Front coils: 24.8 × 10.2 3 Back coils: 24.5 × 11.7	SSFP 2D, 342 cardiac images SSFP 3D, 6 cardiac images	[263–377]	72.4
		SSFP 3D, 6 phantom images	[499–499]	96.2

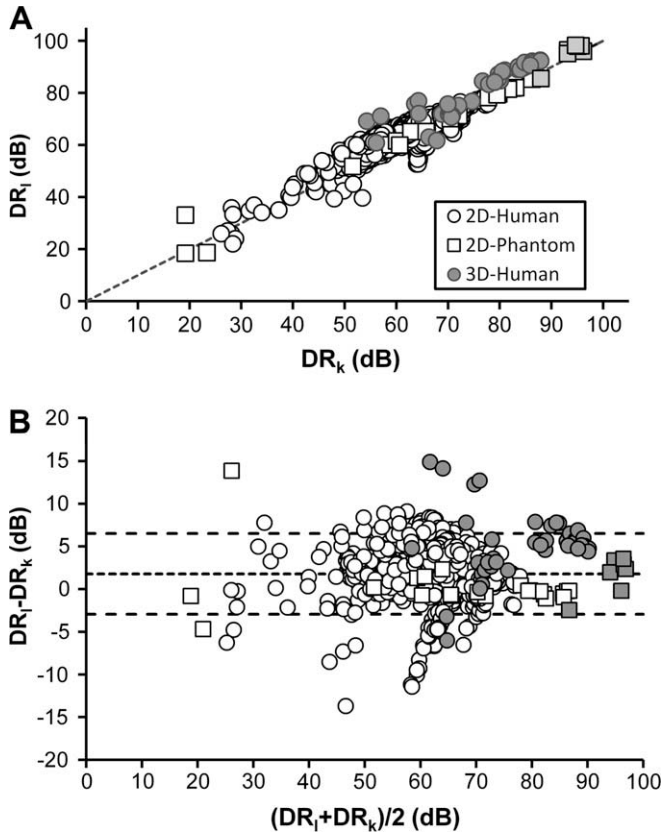

Fig. 3. (A) The DR estimated from the k-space signal (DR_k) and from magnitude images (DR_I) calculated for 1806 images/volumes. Data from 2D and 3D cases and from human and phantom are labeled differently. The solid line is the line of identity. (B) Bland-Altman plot of the difference between DR_I and DR_k vs. their mean value. Mean ± SD for the data is 1.8 ± 2.4 dB. The middle dotted line represents the mean and the top and bottom dashed lines represent mean +2SD and mean −2SD, respectively.

dard 2D and 3D MRI pulse sequences (Table 1), and found it generally to be below 90 dB. The data were acquired from many regions of a normal adult, so the maximum DR is expected to increase by no more than a few dB for different, larger subjects. In practice, a 10 dB margin in DR is advisable to account for changes in body size, pulse sequence parameters or any other undetermined factor.

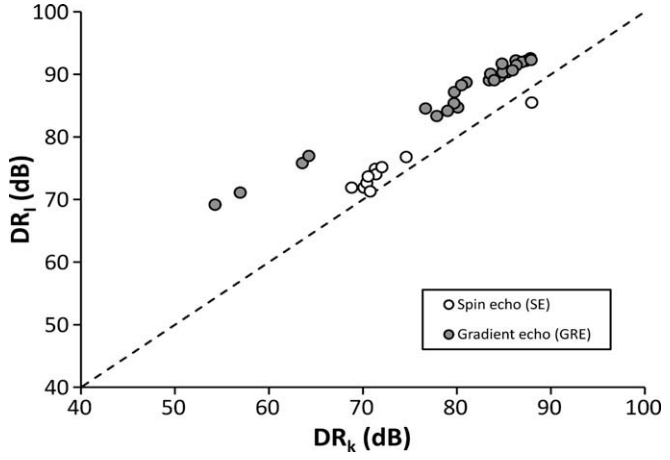

Fig. 4. The DR estimated from the k-space signal (DR_k) and from magnitude images (DR_I) calculated for 3D SE protocols and 3D GRE protocols. Mean difference between DR_I and DR_k for 3D SE protocols is +2 dB while the difference for 3D GRE protocols is +6.8 dB.

Curiously, Fig. 2 shows that the 3D DR is not much greater than the 2D DR. 3D clinical imaging sequences generally use shorter TR, smaller flip angles, larger bandwidths and thinner slices than do 2D sequences. These factors substantially decrease the total amplitude, and thus DR, in the 3D signal relative to what might be expected from the increased sensed volume.

The DR that resulted from applying Eq. (14) to the saved magnitude images was in good agreement with that measured in the raw k-space data as shown in Fig. 3. Thus, Eq. (14) appears to provide a reasonable estimate of DR, provided that the images have not been modified before or after the magnitude operation. Some MRI image processing software applies smoothing filters to the image data. This operation depresses noise and makes the DR appear higher than it really is. If such filters are linear, a scale factor to compensate for the increase in apparent DR can be derived from the FT of the filter kernel.

Section 2.4 showed that DR (in dB) is proportional to the logarithm of the coil radius. Thus, the DR requirements of phased-array MRI receiver channels will decrease (slowly) as the individual detector size is made smaller, for example, to accommodate ever increasing numbers of elements in the same space [1–5]. This also means that system DR is effectively determined by the largest detector coil that is used, notwithstanding the mitigating effects of gradients and/or static field inhomogeneity that may be present over larger sensitive volumes. We also determined that the digitization noise contributed to the system noise figure (NF), when the least significant bit is set equal to the rms noise, is just 0.35 dB.

5.2. Implications for non-coaxial cable signal transmission

In the past few years, a number of research groups have reported efforts to transmit MRI signals from RF coils over optical or wireless links in order to avoid electrical interactions among cables [7–21]. This could be especially helpful with multicoil phased arrays which, as indicated above, at present have as many as 128 cable connections. The DR of routine human images is apparently not as high as has been previously estimated, which means that practical use of optical or wireless links may be more feasible than previously thought. It is important to know the DR requirements for various imaging conditions and the DR of signal transmission links in order to determine whether data transmission via optical or wireless methods is feasible.

The DR of optical links is usually described in terms of spurious-free dynamic range (SFDR), which is the range of input signal power that keeps third-order inter-modulation products below the noise floor [46]. Typical commercial fiber optic systems (e.g. [47]) have SFDR ∼ 100 dB for a 1-Hz bandwidth and a NF of ∼20 dB. Reducing the optical device noise effect to a desirable level of ∼1 dB on the system NF, requires a low noise preamplifier with a gain of about 20 dB.

The net SFDR, including preamplifier and additional bandwidth *BW* in Hz, is given by [46]

$$\mathrm{SFDR}(BW) = \mathrm{SFDR}(1\text{-Hz}) - (2/3)\cdot[NF_t - NF_{link} + G_{preamp} + 10\cdot\log_{10}(BW)] \quad (16)$$

where G_{preamp} is the power gain of the preamplifier, NF_{link} is the noise figure of the optical link and NF_t is the total noise figure of the preamplifier-link cascade, all in dB. The system noise figure is given by the Friis formula [48]

$$NF_t = 10\cdot\log_{10}(nf_t) = 10\cdot\log_{10}\left(nf_{preamp} + \frac{nf_{link}}{g_{preamp} - 1}\right) \quad (17)$$

where nf_{preamp}, nf_{link}, and nf_t are the noise factors of the preamp, the optical link, and the cascade (preamplifier + optical link), respec-

tively and g_{preamp} is the power gain of the preamplifier, all expressed as ratios. The units in decibels are related by

$$NF = 10 \cdot \log_{10}(nf), G = 10 \cdot \log_{10}(g) \quad (18)$$

The total SFDR of the preamplifier and the fiber optic link from the example above is about 66 and 61 dB at a bandwidth of 100 kHz and 500 kHz, respectively. This is significantly less than the 85 dB DR required (including a 10 dB margin) for spine and cardiac arrays. Some recent work on optical fiber links achieved SFDRs of 48–80 dB at 100 kHz bandwidth (Examples 1–7, Table 2). These results are still not compatible with multicoil arrays, especially at high field. Since $SNR \propto B_0$ [49], the DRs at the common clinical field of 1.5 T would only be 6 dB less than that measured here (see Eq. (7)), still too high for linear gain fiber links.

Wei et al. have implemented digital wireless signal transmission [19]. In this case the signal is digitized before being transmitted. This arrangement essentially requires putting an entire receiver module on each coil, which would be difficult at present. Wei et al. also report an SFDR of their wireless system as 89.9 dB at 1 Hz. This is also not good enough to cover the DR needed for bandwidths of 100 kHz or more.

It would appear, then, that fiber optic and wireless links at present by themselves do not have enough DR to transmit raw MRI signals. However, fiber optic and wireless links could be used in conjunction with signal compression, for example, using nonlinear gains [21]. Another approach is to use parallel (linear gain) transmission channels with different gain settings and combine the outputs to effectively produce signal compression [32].

Biber et al. use a VCSEL system (see entry #8 in Table 2) together with signal compression and report a DR of 152 dBc/Hz [21]. This figure represents the range between the noise floor in a 1-Hz bandwidth and the 0.1 dB compression point. dBc/Hz is not readily translated into SFDR so we do not have a direct comparison between their results and the others quoted here. Nevertheless, it would seem that analog fiber optic or wireless links plus compression may be a workable approach toward non-coax MRI signal transmission.

6. Conclusions

We have measured the DR of MRI signals from conventional protocols and have proposed a formula for estimating the DR from magnitude images that shows good agreement with the DR measured in raw signals. From the results in this work, present-day analog fiber optic cables and wireless links by themselves do not appear to provide sufficient DR to transmit MR signals sensed by surface coils in multicoil head, spine, or cardiac arrays at clinical and research static fields of 1.5 T and above. Using these links in combination with signal compression, however, may be practical. Since small coils with limited sensitive regions have a small DR, the trend toward multicoil arrays comprising a large number of small surface coils makes the use of non-electric signal channels increasingly attractive as a way of avoiding detrimental interactions among a large number of coaxial cables.

Acknowledgment

We thank Mr. Ronald Watkins of Stanford University for helpful discussions.

Appendix A. MRI signal digitization and digitization noise (cf. [50], Chapter 9; [51])

Digitizing well above the noise level obviously adds noise. Digitizing at too low a level is a waste of ADC DR. We can characterize the effect of digitization noise as an additional system noise figure. We will show that setting the least significant bit equal to the rms noise value only adds 0.35 dB to the system noise figure. That is the standard we have used for our determination of DR.

The digitization function is given by

$$dig(x) = \delta \cdot \mathrm{round}\left(\frac{x}{\delta}\right) \quad (A1)$$

where δ is the digitization interval and $\mathrm{round}(\frac{x}{\delta})$ is x/δ rounded to the nearest integer. The noise present in the signal channel is Gaussian with a probability density:

$$g(x,\sigma) = \frac{1}{\sigma\sqrt{2\pi}} \exp\left(\frac{-x^2}{2\sigma^2}\right) \quad (A2)$$

where σ is the standard deviation of the noise.

The value of the digitized signal could be anything within $\pm\delta/2$ of the original value, which is commonly modeled as a noise term with a uniform distribution. The probability density function of the total noise in the detected signal is then the convolution of the uniform digitization distribution and the Gaussian noise distribution.

$$p_{noise}(y,\sigma,\delta) = \int_{-\infty}^{\infty} dig(x)g(y-x)dx = \frac{1}{\delta}\int_{-\delta/2}^{\delta/2} dx\, g(y-x) = \frac{1}{2\delta}\left[\mathrm{erf}\left(\frac{y+\delta/2}{\sigma\sqrt{2}}\right) - \mathrm{erf}\left(\frac{y-\delta/2}{\sigma\sqrt{2}}\right)\right] \quad (A3)$$

where erf is the error function. Fig. A1 shows the evaluation of Eq. (A3) for a few values of δ/σ. This is the distribution of true signal

Table 2
Spurious-free dynamic ranges (SFDRs) for fiber optic and wireless link at different values of receiver bandwidth (BW).

Example	Reference	Description	Device SFDR BW = 1 Hz	System SFDR			
				BW = 1 Hz	BW = 10 kHz	BW = 100 kHz	BW = 500 kHz
1.	Yuan et al. [15]	Direct modulationFP laser[1]	–	104.5	77.9	71.2	66.5
2.	Du et al. [18]	Direct modulationFP laser[1]	110.0	103.6	76.9	70.3	65.6
3.	Du et al. [18]	Direct modulation VCSEL laser[2]	116.0	109.6	83.0	76.3	71.6
4.	Du et al. [18]	DFB laser[3]	120.0	113.6	86.9	80.3	75.6
5.	Miteq fiber optic links [47]	Direct modulation DFB laser	106.0	99.9	73.2	66.6	61.9
6.	Memis et al. [20]	Direct modulationDFB laser[3]	–	81.3	54.6	48.0	43.3
7.	Koste et al. [9]	External modulationMZ modulator[4]	–	103.0	76.3	69.7	65.0
8.	Biber et al. [21]	Direct modulationVCSEL with signal compression[5]	–	152 dBc/Hz	–	–	–
9.	Wei et al. [19]	Digital wireless transmission(data at right is the analog SFDR for their wireless circuit)[6]	–	89.9	63.2	56.6	51.9

Notes. (1) FP, Fabry–Perot; (2) VCSEL, vertical cavity surface emitting laser; (3) DFB, distributed Feedback; (4) MZ, Mach Zender; (5) entry 8 is "dBc" (decibels relative to carrier); (6) entry 9 is the analog SFDR for the wireless circuit used by Ref. [19].

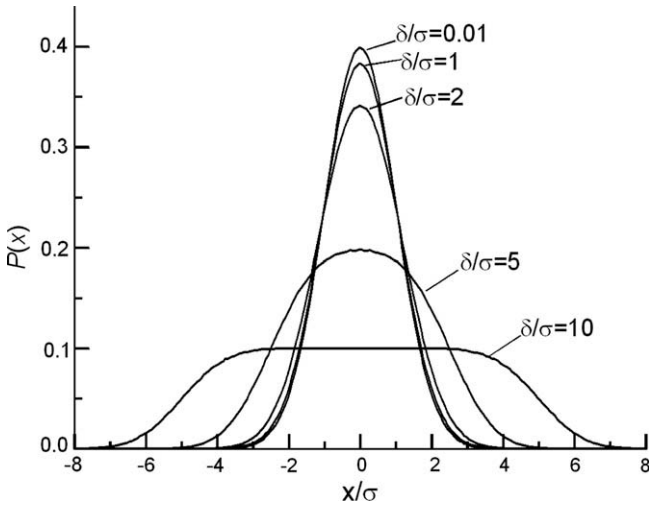

Fig. A1. The probability density function of the noise in the digitized Gaussian signal. δ is the digitization interval and the σ is the standard deviation of the Gaussian noise.

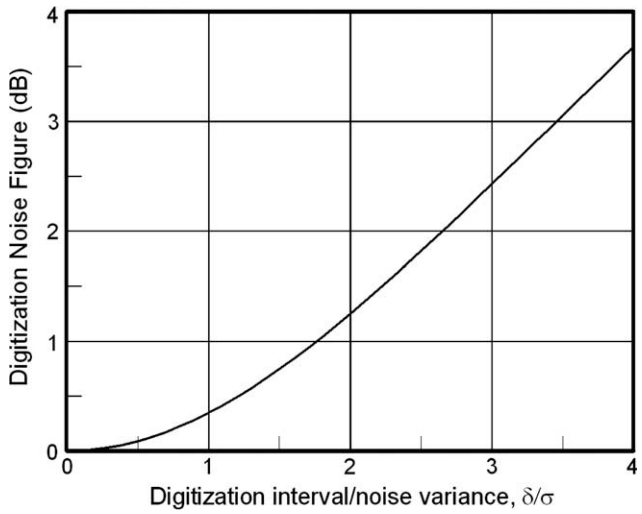

Fig. A2. Digitization noise figure as a function of δ/σ, the ratio of the digitization interval to the noise standard deviation.

relative to the center of the triggered bin. When $\delta/\sigma \approx 0$, i.e. the digitizing interval is much smaller than the noise, the distribution looks like the Gaussian noise. When δ/σ is large, we get a uniform distribution with soft tails.

We can calculate the variance of the joint distribution as

$$\begin{aligned}\mathrm{var}(\delta,\sigma) &= \frac{1}{\delta}\int_{-\infty}^{\infty} dy y^2 \int_{-\delta/2}^{\delta/2} dx\, g(y-x) \\ &= \frac{1}{\delta}\int_{-\delta/2}^{\delta/2} dy \int_{-\infty}^{\infty} dx\, y^2 g(y-x) \end{aligned} \quad \text{(A4)}$$

When Eq. (A4) is integrated we obtain the simple answer

$$\mathrm{var}(\delta,\sigma) = \sigma^2 + \frac{\delta^2}{12} \quad \text{(A5)}$$

In other words, we get the sum of the two variances.

A.1. Digitization noise figure

We can define a *digitization noise figure* (*NFdig*) which tells us the additional noise, in dB, as a function of σ when the signal is digitized.

$$\begin{aligned} NFdig(\delta,\sigma) &= 10\cdot\log_{10}\left(\frac{\mathrm{var}(\delta,\sigma)}{\sigma^2}\right) \\ &= 10\cdot\log_{10}\left[1+\frac{1}{12}\left(\frac{\delta}{\sigma}\right)^2\right] \end{aligned} \quad \text{(A6)}$$

Fig. A2 shows *NFdig* as a function of δ/σ. Table A1 shows a few particular values of *NFdig*. The third column shows the ratio of the digital SNR to the original analog SNR. For example, when $\delta/\sigma = 1$, *NFdig* = 0.35 dB and signal digitization results in an SNR that is 96% of the original analog SNR.

Table A1
Digital noise figure (*NFdig*), i.e. additional noise contributed by digitization. δ/σ is the ratio of digitization interval to rms noise.

δ/σ	*NFdig* (dB)	Amplitude SNR:digital/analog
0.50	0.09	0.98
1.00	0.35	0.96
1.21	0.50	0.94
1.76	1.00	0.89
2.00	1.25	0.87
2.23	1.50	0.84
2.65	2.00	0.79
3.06	2.50	0.75
3.46	3.00	0.71

Appendix B. Dynamic range scaling for circular loop coils

2In the following analysis we derive an estimate of the DR scaling vs. coil size by applying quasi-static low-frequency formulas for the transverse field and sample losses. In this calculation, we use cylindrical coordinates with the z direction along the coil symmetry axis.

B.1. Sample noise power

The noise power generated by a coil is

$$P_N \propto \int_V |\mathbf{A}|^2 dV \quad \text{(B1)}$$

where **A** is the vector potential [52] and the integral is evaluated over the entire volume *V*. The vector potential for a circular loop has only an azimuthal component and is given by [53]

$$\begin{aligned} A_\phi = {} & \frac{\mu I}{\pi}\frac{1}{k(a,\rho,z)}\left(\frac{a}{\rho}\right)^{\frac{1}{2}} \\ & \times\left\{\left(1-\frac{1}{2}[k(a,\rho,z)]^2\right)K([k(a,\rho,z)]^2) - E([k(a,\rho,z)]^2)\right\} \end{aligned} \quad \text{(B2)}$$

where *I* is the current, *a* is the loop radius, ρ and *z* are cylindrical polar radial and *z*-coordinates, μ is medium permeability, $K(\cdot)$ and $E(\cdot)$ are the complete elliptic integral function of the first kind and the second kind, respectively, and

$$[k(a,\rho,z)]^2 = \frac{4a\rho}{[(a+\rho)^2+z^2]} = \frac{4(\frac{\rho}{a})}{[(1+(\frac{\rho}{a}))^2+(\frac{z}{a})^2]} \quad \text{(B3)}$$

Note that A_ϕ (Eq. (B2)) is only a function of the normalized variables $(\frac{\rho}{a})$ and $(\frac{z}{a})$. Thus, we can transform the integral Eq. (B1) as follows:

$$\begin{aligned} P_N &\propto \int_V |\mathbf{A}(a,\rho,z)|^2 2\pi\rho\cdot d\rho dz \\ &= a^3\cdot\int_V \left|\mathbf{A}\left(1,\frac{\rho}{a},\frac{z}{a}\right)\right|^2\cdot 2\pi\left(\frac{\rho}{a}\right)\cdot d\left(\frac{\rho}{a}\right)d\left(\frac{z}{a}\right) \end{aligned} \quad \text{(B4)}$$

Since the final integral is independent of coil diameter, it follows that noise power [52]

$$P_N \propto a^3. \quad \text{(B5)}$$

B.2. Loop coil signal

We next sum the signals that we would receive in the circular coil. According to the reciprocity rule [54], we sum the fields. Considering symmetry, we really want to sum the z-component of the field B_z. B_z is given by [53]

$$B_z = \frac{\mu I}{2\pi}\frac{1}{[(a+\rho)^2+z^2]^{\frac{1}{2}}} \times\left\{K([k(a,\rho,z)]^2)+\left(\frac{a^2-\rho^2-z^2}{(a-\rho)^2+z^2}\right)E([k(a,\rho,z)]^2)\right\} \tag{B6}$$

To convert B_z to a reduced form, i.e., a function of $(\frac{\rho}{a})$ and $(\frac{z}{a})$, adjusting the prefactor obtains:

$$B_z = \frac{1}{a}\cdot\frac{\mu I}{2\pi}\frac{1}{\left[\left(1+\frac{\rho}{a}\right)^2+\left(\frac{z}{a}\right)^2\right]^{\frac{1}{2}}} \times\left[K\left(\left[k\left(1,\frac{\rho}{a},\frac{z}{a}\right)\right]^2\right)+\left(\frac{1-\left(\frac{\rho}{a}\right)^2-\left(\frac{z}{a}\right)^2}{\left(1-\frac{\rho}{a}\right)^2+\left(\frac{z}{a}\right)^2}\right)E\left(\left[k\left(1,\frac{\rho}{a},\frac{z}{a}\right)\right]^2\right)\right] \tag{B7}$$

Then, for the signal sum we have

$$S\propto\int_V B_z(a,\rho,z)dV=\frac{1}{a}\int_V F\left(\frac{\rho}{a},\frac{z}{a}\right)\cdot 2\pi\rho d\rho dz = a^2\int_V F\left(\frac{\rho}{a},\frac{z}{a}\right)\cdot 2\pi\left(\frac{\rho}{a}\right)d\left(\frac{\rho}{a}\right)d\left(\frac{z}{a}\right) \tag{B8}$$

where $F(\frac{\rho}{a},\frac{z}{a})$ is purely a function of the reduced coordinates.

Since the final integral is dimensionless, we now have

$$S\propto a^2. \tag{B9}$$

B.3. Dynamic range scaling

The dynamic range (DR) is proportional to the ratio of the square of S divided by P_N. So

$$\mathrm{DR}=10\cdot\log_{10}\left(\frac{S^2}{P_N}\right)\propto\log_{10}(a). \tag{B10}$$

References

[1] P.J. Ledden, A. Mareyam, S. Wang, P. van Gelderen, J.H. Duyn, 32 Channel receive-only SENSE array for brain imaging at 7 T, in: ISMRM 15th Annual Conference, Berlin, Germany, 2007, p. 242.

[2] M.P. McDougall, S.M. Wright, 64-Channel array coil for single echo acquisition magnetic resonance imaging, Magn. Reson. Imaging 54 (2005) 386–392.

[3] G.C. Wiggins, V. Alagappan, A. Potthast, M. Schmitt, C.J. Wiggins, H. Fischer, K. Jahns, T. Benner, J. Polimeni, L.L. Wald, Design optimization and SNR performance of 3 T 96 channel phased array head coils, in: ISMRM 15th Annual Conference, Berlin, Germany, 2007, p. 243.

[4] C.J. Hardy, R.O. Giaquinto, J.E. Piel, K.W. Rohling, L. Marinelli, E.W. Fiveland, C.J. Rossi, K.J. Park, R.D. Darrow, R.D. Watkins, T.K. Foo, 128-Channel body MRI with flexible high density receiver coil array, in: ISMRM 15th Annual Conference, Berlin, Germany, 2007, p. 244.

[5] M. Schmitt, A. Potthast, D.E. Sosnovik, J.R. Polimeni, G.C. Wiggins, C. Triantafyllou, L.L. Wald, A 128-channel receive-only cardiac coil for highly accelerated cardiac MRI at 3 Tesla, Magn. Reson. Med. 59 (2008) 1431–1439.

[6] Y. Zhu, C.J. Hardy, D.K. Sodickson, R.O. Giaquinto, C.L. Dumoulin, G. Kenwood, T. Niendorf, H. Lejay, C.A. McKenzie, M.A. Ohliger, Highly parallel volumetric imaging with a 32-element RF coil array, Magn. Reson. Med. 52 (2004) 869–877.

[7] E.B. Boskamp, Wireless RF Module for an MR Imaging System, USA patent 2003/0206019 A1, 2003, GE.

[8] M. Konings, S. Weiss, Optical MR Signal Transmission, USA patent 20040226801, Philips, 2004.

[9] G.P. Koste, R.L. Frey, M.C. Nielsen, T.R. Tolliver, R.D. Watkins, Magnetic resonance imaging, a commercial application for analog photonics, in: IEEE Conference on Avionics Fiber-Optics and Photonics, Minneapolis, MN, USA, 2005, pp. 64–65.

[10] G.P. Koste, M.C. Nielsen, T.R. Tolliver, R.L. Frey, R.D. Watkins, Optical MR receive coil array interconnect, in: ISMRM 13th Annual Meeting, Miami Beach, FL, USA, 2005, p. 411.

[11] G. Scott, K. Yu, Wireless transponders for RF coils: system issues, in: ISMRM 13th Annual Meeting, Miami Beach, FL, USA, 2005, p. 330.

[12] S.B. Bulumulla, G.A. Forman, Optical Link for Transmitting Data Through Air from a Plurality of Receiver Coils in a Magnetic Resonance Imaging System, USA patent 7173426 B1, 2006, GE.

[13] J. Wei, B. Wu, J. Yuan, G.X. Shen, Digital Wireless transmission for MRI, in: ISMRM 14th Annual Conference, Seattle, WA, USA, 2006, p. 3542.

[14] J. Yuan, J. Wei, G.X. Shen, Noise figure and dynamic range optimization in optical links for MRI applications, in: ISMRM 14th Annual Conference, Seattle, WA, USA, 2006, p. 2031.

[15] J. Yuan, J. Wei, G. Shen, A direct modulated optical link for MRI RF receive coil interconnection, J. Magn. Reson. 189 (2007) 130–138.

[16] J. Yuan, J. Wei, G.X. Shen, Investigation of dynamic range requirement for MRI signal transmission by optical fiber link, in: ISMRM 15th Annual Conference, Berlin, Germany, 2007, p. 995.

[17] J. Yuan, J. Wei, G.X. Shen, A direct modulated optical fiber link for 0.3 T MRI, in: ISMRM 15th Annual Conference, Berlin, Germany, 2007, p. 322.

[18] C. Du, J. Yuan, G.X. Shen, Comparison of FP, VCSEL and DFB laser diode in optical transmission for MR RF coil array, in: ISMRM 15th Annual Conference, Berlin, Germany, 2007, p. 1041.

[19] J. Wei, Z.G. Liu, Z. Chal, J. Yuan, J.Y. Lian, G.X. Shen, A realization of digital wireless transmission for MRI signals based on 802.11b, J. Magn. Reson. 186 (2007) 358–363.

[20] O.G. Memis, Y. Eryaman, O. Aytur, E. Atalar, Miniaturized fiber-optic transmission system for MRI signals, Magn. Reson. Med. 59 (2008) 165–173.

[21] S. Biber, P. Baureis, J. Bollenbeck, P. Hocht, H. Fischer, Analog optical transmission of 4 MRI receive channels with high dynamic range over one single optical fiber, in: ISMRM 16th Annual Conference, Toronto, Ontario, Canada, 2008, p. 1120.

[22] J. Overweg, in: H. Fujita, R. Bowtell, (Eds.), ISMRM 13th Annual Conference, MR Engineering Study Group, State-of-the-Art Wireless and Fiber Optic Cabling Technologies, Miami, FL, USA, 2005.

[23] A. Reykowski, in: H. Fujita, R. Bowtell, (Eds.), ISMRM 13th Annual Conference, MR Engineering Study Group, State-of-the-Art Wireless and Fiber Optic Cabling Technologies, Miami, FL, USA, 2005.

[24] W. He, X. Qin, R. Jiejing, L. Gengying, Four-channel magnetic resonance imaging receiver using frequency domain multiplexing, Rev. Sci. Instrum. 78 (2007) 015102.

[25] R. Behin, J. Bishop, R.M. Henkelman, Dynamic range requirements for MRI, Concepts Magn. Reson. Part B 26B (2005) 28–35.

[26] V.J. Wedeen, Y.S. Chao, J.L. Ackerman, Dynamic range compression in MRI by means of a nonlinear gradient pulse, Magn. Reson. Med. 6 (1988) 287–295.

[27] A.A. Maudsley, Dynamic range improvement in NMR imaging using phase scrambling, J. Magn. Reson. 76 (1988) 287–305.

[28] D. Idiyatullin, C. Corum, J.Y. Park, M. Garwood, Fast and quiet MRI using a swept radiofrequency, J. Magn. Reson. 181 (2006) 342–349.

[29] K. Kose, K. Endoh, T. Inouye, Nonlinear amplitude compression in magnetic resonance imaging: quantization noise reduction and data memory saving, IEEE Aerospace Electron. Syst. Mag. 5 (1990) 27–30.

[30] M.A. Delsuc, J.Y. Lallemand, Improvement of dynamic range in NMR by oversampling, J. Magn. Reson. 69 (1986) 504–507.

[31] M.A. Elliott, E.K. Insko, R.L. Greenman, J.S. Leigh, Improved resolution and signal-to-noise ratio in MRI via enhanced signal digitization, J. Magn. Reson. 130 (1998) 300–304.

[32] Y. Otake, K. Kose, T. Haish, A solution to the dynamic range problem in MRI using a parallel image acquisition, Concepts Magn. Reson. Part B 29B (2006) 161–167.

[33] W.A. Edelstein, P.A. Bottomley, L.M. Pfeifer, A signal-to-noise calibration procedure for NMR imaging systems, Med. Phys. 11 (1984) 180.

[34] M.J. Firbank, A. Coulthard, R.M. Harrison, E.D. Williams, A comparison of two methods for measuring the signal to noise ratio on MR images, Phys. Med. Biol. 44 (1999) N261–N264.

[35] H. Gudbjartsson, S. Patz, The Rician distribution of noisy MRI data, Magn. Reson. Med. 34 (1995) 910–914.

[36] M.A. Bernstein, D.M. Thomasson, W.H. Perman, Improved detectability in low signal-to-noise ratio magnetic resonance images by means of phase corrected real reconstruction, Med. Phys. 16 (1989) 813–817.

[37] J. Sijbers, A.J. den Dekker, Maximum likelihood estimation of signal amplitude and noise variance from MR data, Magn. Reson. Med. 51 (2004) 586–594.

[38] J. Sijbers, A.J. den Dekker, E. Raman, D. Van Dyck, Parameter estimation from magnitude MR images, Int. J. Imaging Syst. Technol. 10 (1999) 109–114.

[39] J. Sijbers, A.J. den Dekker, P. Scheunders, D. Van Dyck, Maximum-likelihood estimation of Rician distribution parameters, IEEE Trans. Med. Imaging 17 (1998) 357–361.

[40] J. Sijbers, A.J. den Dekker, J. Van Audekerke, M. Verhoye, D. Van Dyck, Estimation of the noise in magnitude MR images, Magn. Reson. Imaging 16 (1998) 87–90.

[41] L. Kaufman, D.M. Kramer, L.E. Crooks, D.A. Ortendahl, Measuring signal-to-noise ratios in MR imaging, Radiology 173 (1989) 265–267.

[42] C.G. Koay, P.J. Basser, Analytically exact correction scheme for signal extraction from noisy magnitude MR signals, J. Magn. Reson. 179 (2006) 317–322.

[43] A.H. Andersen, On the Rician distribution of noisy MRI data, Magn. Reson. Med. 36 (1996) 331–333.

[44] G. McGibney, M.R. Smith, An unbiased signal-to-noise ratio measure for magnetic resonance images, Med. Phys. 20 (1993) 1077–1078.
[45] J.M. Bland, D.G. Altman, Statistical methods for assessing agreement between two methods of clinical measurement, Lancet 1 (1986) 307–310.
[46] C.H. Cox, Analog Optical Links: Theory and Practice, second ed., Cambridge University Press, 2004.
[47] Miteq Fiber Optic Links, 2007. Available from: <http://www.miteq.com/components/fiber_optic.htm/>.
[48] J.S. Chitode, Communication Theory, Technical Publications, Pune, India, 2006.
[49] W.A. Edelstein, G.H. Glover, C.J. Hardy, R.W. Redington, The intrinsic signal-to-noise ratio in NMR imaging, Magn. Reson. Med. 3 (1986) 604–618.
[50] J.D. Gibson, Principals of Digital and Analog Communications, Macmillan, New York, NY, USA, 1989.
[51] B. Widrow, I. Kollar, M.-C. Liu, Statistical theory of quantization, IEEE Trans. Instrum. Meas. 45 (1996) 353–361.
[52] W.A. Edelstein, T.H. Foster, J.F. Schenck, The relative sensitivity of surface coils to deep lying tissues, in: 4th Annual Meeting, Society of Magnetic Resonance, London, 1985, pp. 964–965.
[53] W.R. Smythe, Static and Dynamic Electricity, McGraw-Hill, New York, 1950.
[54] D.I. Hoult, P.C. Lauterbur, The sensitivity of the zeugmatographic experiment involving human samples, J. Magn. Reson. 34 (1979) 425–433.